HHS Public Access

Author manuscript

Exp Eye Res. Author manuscript; available in PMC 2022 May 01.

Published in final edited form as:

Exp Eye Res. 2021 May ; 206: 108536. doi:10.1016/j.exer.2021.108536.

Differences in the properties of porcine cortical and nuclear fiber cell plasma membranes revealed by saturation recovery EPR spin labeling measurements

Natalia Stein[*], **Witold K. Subczynski**[*]

Department of Biophysics, Medical College of Wisconsin, 8701 Watertown Plank Road, Milwaukee, WI 53226, USA

Abstract

Eye lens membranes are complex biological samples. They consist of a variety of lipids that form the lipid bilayer matrix, integral proteins embedded into the lipid bilayer, and peripheral proteins. This molecular diversity in membrane composition induces formation of lipid domains with particular physical properties that are responsible for the maintenance of proper membrane functions. These domains can be, and have been, effectively described in terms of the rotational diffusion of lipid spin labels and oxygen collision with spin labels using the saturation recovery (SR) electron paramagnetic resonance method and, now, using stretched exponential function for the analysis of SR signals. Here, we report the application of the stretched exponential function analysis of SR electron paramagnetic resonance signals coming from cholesterol analog, androstane spin label (ASL) in the lipid bilayer portion of intact fiber cell plasma membranes (IMs) isolated from the cortex and nucleus of porcine eye lenses. Further, we compare the properties of these IMs with model lens lipid membranes (LLMs) derived from the total lipids extracted from cortical and nuclear IMs. With this approach, the IM can be characterized by the continuous probability density distribution of the spin-lattice relaxation rates associated with the rotational diffusion of a spin label, and by the distribution of the oxygen transport parameter within the IM (*i.e.*, the collision rate of molecular oxygen with the spin label). We found that the cortical and nuclear LLMs possess very different, albeit homogenous, spin lattice relaxation rates due to the rotational diffusion of ASL, indicating that the local rigidity around the spin label in nuclear LLMs is considerably greater than that in cortical LLMs. However, the oxygen transport parameter around the spin label is very similar and slightly heterogenous for LLMs from both sources. This heterogeneity was previously missed when distinct exponential analysis was used. The spin lattice relaxation rates due to either the rotational diffusion of ASL or the oxygen collision with the spin label in nuclear IMs have slower values and wider distributions compared with those of cortical IMs. From this evidence, we conclude that lipids in nuclear IMs are less fluid and more heterogeneous than those in cortical membranes. Additionally, a comparison of

[*]Corresponding Authors: Natalia Stein, Department of Biophysics, Medical College of Wisconsin, 8701 Watertown Plank Road, Milwaukee, WI 53226, USA; Tel: (414) 955-4044; nstein@mcw.edu Witold K. Subczynski, Department of Biophysics, Medical College of Wisconsin, 8701 Watertown Plank Road, Milwaukee, WI 53226, USA; Tel: (414) 955-4038; subczyn@mcw.edu.

properties of IMs with corresponding LLMs, and lipid and protein composition analysis, allow us to conclude that the decreased lipid-to-protein ratio not only induces greater rigidity of nuclear IMs, but also creates domains with the considerably decreased and variable oxygen accessibility. The advantages and disadvantages of this method, as well as its use for the cluster analysis, are discussed.

Graphical Abstract

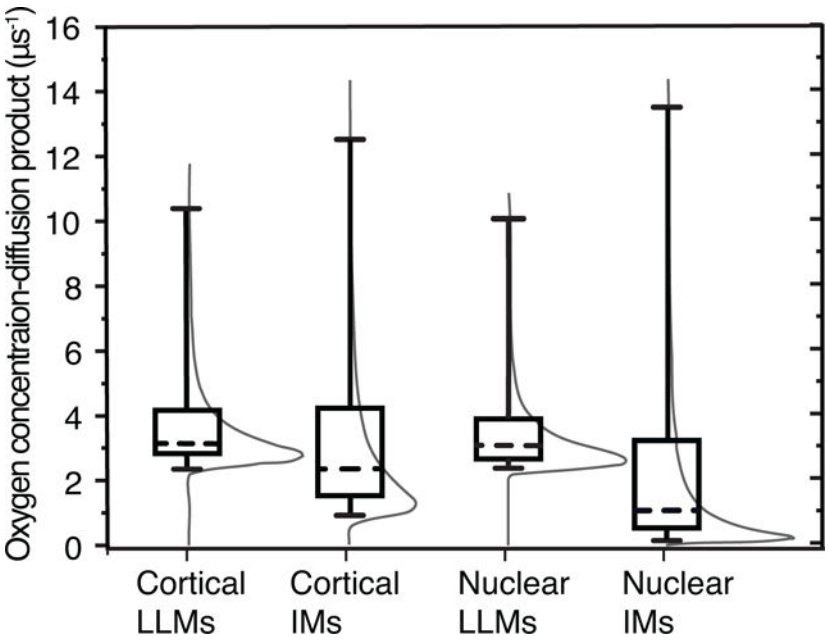

Keywords

stretched exponential; membrane fluidity; membrane heterogeneity; saturation recovery EPR; spin label; eye lens

1. Introduction

The application of the saturation recovery (SR) electron paramagnetic resonance (EPR) technique, with the use of lipid-analog nitroxide spin labels, was focused on studies of the organization and dynamics of lipid bilayer membranes (Altenbach et al., 1989; Kawasaki et al., 2001; Mainali et al., 2017a, 2013b, 2011b; Marsh, 2018; Raguz et al., 2011a, 2011b; Subczynski et al., 2007a, 2007b, 1991; Yin et al., 1987). By fitting the SR signal to exponential function, the spin-lattice relaxation rate (T_1^{-1}, inverse of the spin-lattice relaxation time) can be obtained. The T_1^{-1}, in the absence of other paramagnetic molecules, is determined primarily by the rotational diffusion of the nitroxide moiety of spin labels (Mailer et al., 2005; Marsh, 2018; Robinson et al., 1994), thus giving information about the membrane fluidity sensed by this nitroxide moiety. Using phospholipid (PL) and cholesterol (Chol) analog spin labels (*i.e.*, probe molecules that mimic the behavior of the parent molecules), the information about rotational motion of PLs and Chol can be obtained.

Introduction of the relaxation paramagnetic agent, molecular oxygen, into investigated membranes (by equilibrating them with the controlled partial pressure of oxygen) tremendously increased the application of the SR EPR methods to study membrane organization and dynamics. Use of this approach allowed us, for the first time, to evaluate the oxygen permeability coefficient across model (Mainali et al., 2013b; Raguz et al., 2008; Subczynski et al., 1991, 1989; Widomska et al., 2007) and biological membranes (Raguz et al., 2015a; Subczynski et al., 1992; W. K. Subczynski et al., 2017). It also allowed discrimination of membrane domains in model (Ashikawa et al., 1994; Kawasaki et al., 2001; Mainali et al., 2015, 2013c, 2013b; Raguz et al., 2011a, 2011b, 2008; Subczynski et al., 2010, 2007a; Widomska et al., 2007; Wisniewska and Subczynski, 2008) and biological membranes (Raguz et al., 2015a, 2014), which cannot be discriminated by spin labels alone. The spin-label oximetry approach was used to monitor membrane fluidity the diffusion of small probe molecules within the membrane, namely, diffusion of molecular oxygen. The profiles of the oxygen diffusion-concentration product across membranes that we obtained are new and very informative; they provide a sensitive way to describe membrane fluidity and, importantly, the neighboring lipid non-conformability.

Recently, we advanced the SR EPR approach for membrane studies by introducing the new way to analyze the SR signals using stretched exponential function (SEF) (Stein and Subczynski, 2020). To the best of our knowledge, this was the first time SEF was used to analyze SR EPR signals of spin-labeled biological membranes. This approach removes the requirement for a specific number of exponential components in the SR signal, each of which is characterized by the strict spin lattice relaxation rate and assigned to a distinct homogeneous membrane domain. With only two fitting parameters (the characteristic spin-lattice relaxation rate and the heterogeneity parameter), the analysis of SR signals with SEF offers a way to construct a continuous probability distribution of all possible spin lattice relaxation rates rather than indicating two or three strict distinct exponentials. The probability of finding a range of spin lattice relaxation rates associated with particular domains or neighboring lipids can be evaluated.

In our first paper (Stein et al., 2019), we applied the SEF to analyze SR signals for spin-labeled complex biological membranes (cortical and nuclear fiber cell plasma membranes of the porcine eye lenses) when the probability distributions of spin-lattice relaxation rates were determined only by the rotational diffusion of spin labels. These conditions were achieved for deoxygenated membrane samples. We demonstrated that the rates and the rate distributions sensed by PL analog spin labels (12-SASL) and Chol analog androstane spin labels (ASL) are faster and narrower in cortical membranes as compared with those measured in nuclear membranes. Constructed probability distribution functions and cumulative distribution functions allowed us to conclude that ~40% of PL molecules and ~25% of Chol molecules in nuclear membranes have rotational diffusions slower than those encountered in cortical membranes. Thus, in nuclear membranes, a very rigid environment exists that is not seen in cortical membranes. In that paper, we introduced the rescaling procedure that allowed construction of probability distribution functions and cumulative distribution functions with the x-axis expressed as T_1^{-1}, which allowed a simple and straightforward analysis of the data obtained for each membrane sample with its individual characteristic relaxation times and stretching parameters. Finally, we showed that the

stretched exponential parameters can be used to determine the significance of experimental differences and to cluster the samples based on origin using a K-means clustering analysis that is useful in exploratory research.

In our second publication (Stein and Subczynski, 2020), we advanced the previously established spin label SR EPR methods with the use of the SEF analysis to the case where the second relaxation process, namely the Heisenberg exchange between the spin label and molecular oxygen that occurs during bimolecular collisions, contributes to the decay of SR signals. We developed the theory and formulated basic equations for the analysis of SR EPR signals using SEF in membranes equilibrated with air, which allowed separate construction of probability distributions of spin-lattice relaxation rates determined by the rotational diffusion of spin labels, and the distribution of relaxations induced strictly by collisions with molecular oxygen. The latter distribution is determined by the distribution of the oxygen diffusion-concentration product within the membrane, which forms a new way to describe membrane fluidity and heterogeneity. We demonstrated the application of these new approaches, using intact fiber cell plasma membranes (IMs) of the cortex and nucleus of porcine eye lenses and lens lipid membranes (LLMs) prepared from the total lipid extract from these IMs, both labeled with ASL. These investigations clearly showed the extent to which integral and peripheral membrane proteins decrease the fluidity and increase the heterogeneity of membrane fluidity sensed by the Chol analog ASL alone and sensed by the movement and solubility of molecular oxygen. They also demonstrated that molecular oxygen is a very sensitive probe molecule for such investigations.

Here, we applied the above described approaches for the analysis of the SR EPR data with the application of the SEF to compare properties of membranes from different origins, namely IMs isolated from the cortex and nucleus of two-year-old porcine eye lenses. We also compared properties of these complex IMs with appropriate LLMs prepared from the total lipid extracts from IMs. For these investigations, we chose ASL. This work, in which we further developed and tested the method of analysis SR EPR signals with SEF approach, completes the research discussed our previous two papers (Stein et al., 2019; Stein and Subczynski, 2020).

2. Materials and Methods

Methods developed in (Stein et al., 2019; Stein and Subczynski, 2020) are applied to study differences between IMs isolated from the cortex and nucleus of porcine eye lenses labeled with the Chol analog ASL. These membranes were chosen because they were previously investigated in detail using both continuous wave (CW) and SR EPR approaches (Mainali et al., 2018, 2012a; Raguz et al., 2015b, 2008). Also, new methodologies for applying the SEF to analyze SR signals were first demonstrated on these membranes. Because of that, in the sections below, we only briefly describe all necessary procedures for samples preparations and handlings, referring readers to appropriate references. We provide the detailed procedures and indicated equations needed for the analysis of SR signals with SEF.

2.1. Materials

Spin-labeled Chol analog (*i.e.*, ASL) was purchased from Molecular Probes (Eugene, OR) (see the structures in Fig. 2 of Ref. (Witold K Subczynski et al., 2017)). Other chemicals, of at least reagent grade, were purchased from Sigma-Aldrich (St. Louis, MO).

2.2. Isolation of IMs and total lipids from cortical and nuclear samples

These procedures are described in (Stein and Subczynski, 2020). Porcine eyes were obtained on the day of slaughter from Johnsonville Sausage, LLC (Watertown, WI). Lenses were dissected and kept at −80°C until needed. For the presented experiments, 36 lenses were thawed and decapsulated, and the cortex, the soft outer portion of the lens, was separated from the nucleus, the firm inner portion of the lens (Estrada and Yappert, 2004; Rujoi et al., 2003). Cortical and nuclear IMs were isolated separately (Bloemendal et al., 1972; Cenedella and Fleschner, 1992; Chandrasekher and Cenedella, 1995). First, the fiber cells were homogenized, and the soluble component was removed by centrifugation. Special care was taken to produce a uniform suspension by repeatedly aspirating the insoluble membrane suspension through a syringe fitted with an 18-gauge needle. Half of each sample was aliquoted into 18 different tubes each and stored in −80°C as IMs. The other half of the sample was lyophilized. The dry weights were recorded, and lipids were extracted using Folch methods. The Chol-to-PLs ratio were determined by mass spectrometry at Medical College of Wisconsin the Pharmacology and Toxicology Mass Spectrometer Facility (Milwaukee, WI).

2.3. Spin labeling of IMs

Spin labeling from the dry film of ASL on the bottom of a test tube was performed as described previously (Raguz et al., 2015b). The ASL was introduced as 1 mol% of the total lipid in each sample. IM suspensions were added to the test tubes and shaken for about 2 h at room temperature. Finally, spin-labeled membrane suspensions were centrifuged for a short time, and the loose pellet was transferred to a 0.6 mm i.d. capillary made of gas-permeable methylpentene polymer and used for EPR measurements (Subczynski et al., 2005).

2.4. Preparation of spin-labeled LLMs

Multilamellar dispersions made from the total lipids extracted either from the cortical or the nuclear samples and containing 1 mol% of ASL (*i.e.*, LLMs) were prepared using the rapid solvent exchange method (Mainali et al., 2013b). The final membrane dispersions containing 1 to 2 mg of total lipids were centrifuged briefly (12000 g, 15 min, 4°C), and the loose pellet was used for EPR measurements.

2.7. SR EPR measurements

SR EPR signals were obtained on the central line of the ASL CW EPR spectrum, as indicated by the arrows in Fig. 1, using short-pulse SR EPR at X-band with a loop-gap resonator (Mainali et al., 2017a). The X-band EPR spectrometer with SR capacity was developed at the National Biomedical EPR Center (Milwaukee, WI). Recently, the apparatus received two major hardware improvements: One improvement allows a short (300 ns duration) saturating pulse of 1 W of power to be delivered to the loop-gap resonator, and the

other reduces the dead time after the pump pulse from 300 ns to 100 ns. All measurements were carried out at ~36°C for samples equilibrated with the same gas that was used for temperature control (*i.e.*, a controlled mixture of nitrogen and dry air adjusted with flowmeters [Matheson Gas Products; model 7631H-604]).

2.8. Analysis of SR signals using SEF

The first 120 ns from all recorded signals was removed before the further analysis because of the irregularity of the data. All SR signals were normalized and, using the Levenberg-Marquardt algorithm in the Origin 2020 (Northampton, MA) software package, fitted to Eq. (1):

$$I(\mathrm{t}) = \exp\left(-\left(tT_{1\ \mathrm{strobs}}{}^{-1}\right)^{\beta\mathrm{obs}}, \right. \tag{1}$$

where I(t) is the signal at time t, $T_{1\mathrm{strobs}}{}^{-1}$ is the fitted rate parameter at a particular air fraction, and β_{obs} is the corresponding fitted heterogeneity parameter. The zero time was taken at 220 ns after the pump pulse. Fitted parameters, $T_{1\mathrm{strobs}}{}^{-1}$ and β_{obs}, were obtained for each record. At least three records were used to calculate the averages and standard deviations per each air fraction.

2.8.1. Analysis of SR signals coming from IMs and LLMs—The aversage $T_{1\mathrm{strobs}}{}^{-1}$ values for each sample at various air fractions (f_{Air}) were plotted versus the air fraction at which they were obtained and fitted to Eq. (2):

$$T_{1\ \mathrm{strobs}}{}^{-1} = W_{\mathrm{str}}\, f_{\mathrm{Air}} + T_{1\mathrm{strN2}}{}^{-1}, \tag{2}$$

where W_{str} is the SOTP rate parameter and $T_{1\mathrm{strN2}}{}^{-1}$ is the spin-lattice relaxation rate due to rotational diffusion and should be the same as the observed value obtained experimentally under nitrogen.

The averaged β_{obs} values were also plotted versus the air fraction at which they were obtained. The plots for each sample were fitted to Eq. (3):

$$\beta_{\mathrm{obs}} = \beta_{\mathrm{N2}}\left(T_{\mathrm{strN2}}{}^{-1}/T_{1\ \mathrm{strobs}}{}^{-1}\right) + \beta_{\mathrm{W}}\left(W_{\mathrm{st}} f_{\mathrm{Air}}\, /T_{1\ \mathrm{strobs}}{}^{-1}\right), \tag{3}$$

where β_{N2} is the heterogeneity parameter associated with $T_{1\mathrm{strN2}}{}^{-1}$, and β_{W} is the SOTP heterogeneity parameter.

The probability density distributions and the corresponding cumulative distributions were obtained as described previously (Stein and Subczynski, 2020). The probability density distributions for the given β parameters were computed in MATLAB R2018a (MathWorks, Natick, MA) using Eq. 11 from (Johnston, 2006). The s-values, as defined in(Johnston, 2006), for each distribution were multiplied by the corresponding stretched rate parameter to produce rate values. To maintain normalization of the probability distribution, the density values had to be divided by the same values as the corresponding stretched rates. The cumulative distributions were obtained by integrating the area under the density distribution

from zero to the particular rate. The values of the 5th, 25th, 50th (median), 75th, and 95th percentiles were obtained from the cumulative distributions.

3. Results and Discussion

When we introduce new methods to study lens fiber cell plasma membranes, we test them on IMs from the cortex and nucleus of two-year-old porcine eye lenses before transferring them to studies of human lenses. Here, we show broad applications of the recently developed SR EPR spin labeling approaches with SEF analysis (Stein et al., 2019; Stein and Subczynski, 2020) to compare the properties of IMs isolated from the cortex and nucleus of porcine eye lenses as well as the properties of these IMs with their models, namely LLMs prepared from the total lipid extracts from IMs. The Chol analog ASL is a good choice because this spin label can be easily incorporated into the IMs. Additionally, Chol is the major lipid component of lens fiber cell plasma membranes (Borchman and Yappert, 2010; Deeley et al., 2008; Rujoi et al., 2003).

3.1. Characterization of cortical and nuclear IMs and LLMs

The mean weights and standard deviations of the cortical and nuclear portions from a single lens were roughly the same, 0.432 ± 0.0911 g and 0.461 ± 0.0813 g, respectively. The total wet weights from 36 lenses were 15.6 g for cortical and 16.6 g for nuclear samples. Half of each IM sample was lyophilized, and the total lipids were extracted providing us with the weights of proteins and lipids in the IMs. The dry weights of cortical and nuclear lyophilize IMs were 0.0637 g and 0.199 g, respectively, whereas the total lipids from the cortical and nuclear IMs weighed 12.1 mg and 7.50 mg, respectively. The dry membrane component of fiber cells, which includes peripheral and integral membrane proteins and the bilayer lipids, comprises 0.816% and 2.40% of the total cortical and nuclear fiber cell wet weights, respectively. This is consistent with the well-documented observation that fiber cells undergo compaction and lose water as they age, with the least water found in the center of the lens (Bassnett and Costello, 2017). Additionally, the proteins account for 81% and 96% of the cortical membrane and nuclear membrane dry weights, respectively. For comparison, the protein in the red blood cell membranes comprises only 44% of dry weight (Dupuy and Engelman, 2008).This increase is consistent with the previously published data, indicating that as fiber cells age certain phospholipids are depleted (Estrada and Yappert, 2004; Yappert et al., 2003) and previously soluble proteins bind to the membranes with higher affinity(Chandrasekher and Cenedella, 1995; Su et al., 2011; Truscott et al., 2011; Wang et al., 2013).

The Chol-to-PL ratios were found to be 0.60 and 2.7 in cortical and nuclear membranes, with an average PL weight of 744 Da. Given that these ratios and the amounts of lipids extracted from each subsection, the cortical and nuclear membranes contained 12.4 μmoles and 4.19 μmoles, respectively, of PLs for the total of 16.59 μmoles in the whole lens. Chol accounts for 7.42 μmoles and 11.3 μmoles in cortical and nuclear membranes, respectively, for the total of 19.02 μmoles in a whole lens. The Chol-to-PL ratio in the whole lens is 1.14. These results are slightly lower than those published by (Deeley et al., 2008), where the approximate Chol-to-PL mole ratio for porcine membranes can be calculated to be

approximately 1.4 for the whole lens. In addition, we can conclude that lipid-to-protein mole ratio decreases from 11.5 in cortical membranes to 2.42 in nuclear membranes, assuming the average protein weight is 30 kDa. The PL-to-protein mole ratio changes from 7.21 in cortical membranes to 0.657 in nuclear membranes. Similar trend, although not as pronounced, is observed in for cholesterol 4.31 in cortical and 1.77 in nuclear IMs.

It is important to note that the assumed average protein molecular weight above is a rough estimate. The intact eye lens membranes are complex in their protein composition (Bassnett and Costello, 2017; Song et al., 2009). For instance, aquaporine-0 is considered to be the major integral membrane protein with a full molecular weight of about 28 kDa. However, this protein is prone to cleavage and truncations that generates smaller fragments (Korlimbinis et al., 2009; Wenke et al., 2015). While it comprises a detectable amount in membranes isolated from younger human lenses, aquaporin-0 is barely detectable in membranes isolated from older lenses partly due to truncation and partly due to comprising smaller fraction due to crystallin binding (Truscott et al., 2011). Connexins 46 and 50 are 46 kDa and 50 kDa, respectively, form another major type of integral membrane protein. These proteins seem to be depleted with age and are missing in senile cataractous lenses (Buzhynskyy et al., 2011). But the majority of the protein as isolated in native or in partially urea stripped membranes is crystallin protein that becomes water insoluble with age (Chandrasekher and Cenedella, 1995; Truscott et al., 2011).

3.2. CW spectra and SR signals of ASL in cortical and nuclear IMs and LLMs

For brevity, the maximum splitting between the outermost peaks obtained directly from the CW EPR spectra of ASL (see inserts in Fig. 1) was used as a convenient parameter to monitor the order parameter of anisotropic motion of ASL (Hubbell and McConnel, 1971). The wobbling motion generates an angular distribution of the long axis of ASL molecules within the confines of a cone imposed by the membrane environment and the order parameter indicates the amplitude of that wabbling motion. However, it is often used to monitor membrane fluidity as was done by Kusumi et al. (Kusumi et al., 1986) (a greater maximum splitting indicates lower membrane fluidity). Maximum splitting in cortical (Fig. 1A) and nuclear (Fig. 1B) LLMs are 37.7 G and 39 G, respectively, which reflects the greater Chol content and the greater ordering effect of Chol in nuclear LLMs. The maximum splitting in the EPR spectrum of cortical IMs (Fig. 1A') increases only slightly, by 0.3 G, as compared with that in cortical LLM (Fig. 1A), indicating that the presence of proteins and their organization in these membranes does not affect ASL order as detected by CW EPR. It can be partly explained by the fact that Chol molecules as well as their analog ASL are substantially excluded from boundary lipids surrounding integral membrane proteins (Bieri and Hoelzl Wallach, 1975; Warren et al., 1975), or that the residence time of the ASL at the protein boundary is so short that no specific interactions are detected in cortical IMs (Páli and Kóta, 2019)

The CW EPR spectrum of ASL in nuclear IMs (Fig. 1B') is very different than that in cortical IMs (Fig. 1A'). It shows two clear components indicated by two maximum splitting. As noted in our previous publications (Mainali et al., 2012a; Raguz et al., 2015b), the greater maximal splitting is the characteristic of the strongly immobilized ASL and indicates the

presence of very rigid environment for Chol molecules existing in nuclear IMs with the exchange rate with bulk lipids slower than the time scale of CW method. The values of two maximum splitting in nuclear IMs are 40 G and 61 G, respectively, close to values estimated earlier for similar membranes (Mainali et al., 2012a; Raguz et al., 2015b). We assigned the strongly immobilized component as coming from ASL molecules trapped within aggregates and arrays of integral membrane proteins or otherwise immobilized by the presence of side chains on the partially inserted peripheral proteins. Our recent unpublished data indicate that the immobilized component in the EPR spectrum of ASL observed in nuclear IMs disappears upon treatment with 8 M urea. We concluded that the presence of peripheral proteins creates a highly immobile lipid environment, with the slow ASL exchange rate with other domains, or that the partially inserted, unfolded peripheral proteins or truncated peptide (Grami et al., 2005; Tang and Borchman, 1998) form rigid complexes with ASL. Interestingly, that similar pattern is observed for human IMs.

The immobilized component in the EPR spectra of ASL coming from cortical IMs appears only for membranes isolated from the lenses of 60- to 80-year-old donors (Raguz et al., 2015a). The immobilized component is always present in nuclear IMs from lenses of donors of all ages. These introductory data indicate that both porcine eye lens membranes and ASL as a monitoring molecule are good system to present the abilities of the SR EPR SEF methods.

3.3. Application of SEF to fit SR signals and obtain SEF parameters

3.3.1. Rotational diffusion in LLMs—Fig. 1 presents the procedure of fitting the representative SR signals coming from ASL in cortical and nuclear IMs and LLMs, recorded after deoxygenation, and after equilibration with 50% air, to the SEF using Eq. (1). Based on the residuals, both signals obtained under nitrogen and 50% air fit well to Eq. (1). Such experiments were performed for membranes equilibrated with various air fractions from 0% to 100%. These procedures allow the SEF fitting parameters $T_{1\mathrm{strobs}}{}^{-1}$ and β_{obs} to be obtained for all SR signals analyzed with the SEF. The cumulative data for the obtained parameters are presented in Fig. 2 as a function of the air fraction in the equilibrating gas mixture.

It is important to note that, in the magnetically diluted deoxygenated samples, the spin lattice relaxation rates were determined primarily by the rotational diffusion of spin labels, and the $T_1{}^{-1}$s are directly proportional to the rotational diffusion rates of spin labels (Mainali et al., 2013a, 2011a). For this reason, the fitting parameters $T_{1\mathrm{strobs}}{}^{-1}$ and β_{obs} obtained under nitrogen are denoted as $T_{1\mathrm{strN2}}{}^{-1}$ and β_{N2}. The averages of these parameters and their standard deviations obtained from at least three signals were found to be $0.564 \pm 2.25 \times 10^{-3}$ μs^{-1} and $0.991 \pm 6.15 \times 10^{-3}$ for cortical LLMs and $0.367 \pm 1.98 \times 10^{-3}$ μs^{-1} and $0.993 \pm 4.15 \times 10^{-3}$ for nuclear LLMs. Because β_{N2} parameters are practically equal to 1, these SR signals represent single exponential decays and $T_{1\mathrm{strN2}}{}^{-1}$s are the same as $T_{1\mathrm{N2}}{}^{-1}$s, single spin lattice relaxation rates that characterize the rotational diffusion of ASL in LLMs. The ASL rotational diffusion is slower in nuclear LLMs as compared with that in cortical LLMs, reflecting the more rigid environment induced by a high Chol-to-PL ratio and the depletion of unsaturated PLs from the nuclear region of the eye lens (Estrada and Yappert,

2004). However, for similar Chol-to-PL ratios, these membranes are significantly more fluid than model membranes made of sphingomyelin-Chol at the same temperature (Mainali et al., 2012b). This may be because the model membranes were made of a single PL, whereas the eye lens contains a mixture of PLs with mixed acyl chains lengths and a degree of unsaturation.

3.3.2 Rotational diffusion in IMs—For IMs, the SEF parameters T_{1strN2}^{-1} and β_{N2} determined for deoxygenated samples are 0.348 ± 2.14 × 10^{-3} μs^{-1} and 0.947 ± 5.75 × 10^{-3} for cortical IMs, and 0.252 ± 2.86 × 10^{-3} μs^{-1} and 0.904 ± 0.011 for nuclear IMs, confirming our previous results (Stein et al., 2019)that, on average, the ASL probes in nuclear membranes are in more rigid environments than those in cortical membranes. The β_{N2} parameters are sufficiently lower than 1, which indicates that the membrane fluidities sensed by ASL in IMs are heterogeneous and should be characterized by the probability distribution of T_{1N2}^{-1}s. Additionally, the β_{N2} value obtained for the nuclear membranes is lower than that obtained for the cortical membranes, confirming a higher heterogeneity of the ASL environment in nuclear membranes than in cortical membranes.

3.3.3. *T_{1str} and the stretching parameter β—effect of molecular oxygen in LLMs—*Cumulative data for $T_{1strobs}^{-1}$ and β_{obs} for cortical and nuclear LLMs for samples equilibrated with different fractions of air are presented in Fig. 2A and B. Recall from Sect. 3.3.1 that the T_{1strN2}^{-1} for cortical LLMs is almost twice as fast as that for nuclear LLMs, which indicates that the rotational diffusion rate of ASL in cortical LLMs is significantly greater than that in nuclear LLMs. As shown in Fig. 2A, in both cortical and nuclear LLMs, the $T_{1strobs}^{-1}$ increases linearly upon addition of air in an equilibrating gas mixture. Despite having such different T_{1strN2}^{-1}, the slopes of these linear dependences are practically the same for both LLMs. The values of $T_{1strobs}^{-1}$ as a function of air fraction were fitted with the linear equation, with an intercept and a slope of 0.529 ± 0.0295 and 3.62 ± 0.136 μs^{-1} for cortical LLMs, respectively, and of 0.367 ± 1.94 × 10^{-3} and 3.43 ± 0.0123 μs^{-1} for nuclear LLMs, respectively. The values following the plus/minus sign indicate the error of fitting. The intercepts are the fitted T_{1strN2}^{-1}s and are very close to those obtained experimentally in Sect. 3.3.1. The slopes are measures of the stretched oxygen transport parameters W_{str}s, which depend on the collision rates of oxygen with ASL and are very similar to each other despite the difference in T_{1strN2}^{-1}s and Chol-to-PL ratios.

The β parameter is essential for stretched exponential analysis of SR signals because it determines the heterogeneity of the distribution of rates. The β_{obs} parameters for cortical and nuclear LLMs are plotted versus the air fractions in Fig. 2B. These values represent the sum of β_{N2} and β_W parameters weighted by their respective rates at a given air fraction (Stein and Subczynski, 2020). The β_Ws were determined by fitting the plots of β_{obs}s for cortical and nuclear LLMs versus the air fractions to Eq. 3 while holding the T_{1strN2}^{-1}s and W_{str}s constant. β_Ws were found to be 0.914 ± 0.033 for cortical LLMs and 0.937 ± 0.012 for nuclear LLMs.

3.3.4. T_{1str} and the stretching parameter β—effect of molecular oxygen in IMs—Cumulative data for $T_{1strobs}^{-1}$ and β_{obs} for cortical and nuclear IMs for samples equilibrated with different fractions of air are presented in Fig. 2C and D. Upon the increase

of the fraction of air in the equilibrating gas mixture, the $T_{1strobs}{}^{-1}$s exhibit amazing linearity with the increase of air fraction in both cortical and nuclear membranes (Fig. 2C). The values of $T_{1strobs}{}^{-1}$ as a function of air fraction were fitted with the linear equation with a slope and a zero intercept of 2.73 ± 0.0581 μs^{-1} and 0.348 ± 0.034 μs^{-1} for cortical IMs, respectively, and of 1.34 ± 0.0345 μs^{-1} and 0.252 ± 3.7×10^{-3} μs^{-1} for nuclear IMs, respectively. The intercept values reflect the $T_{1strN2}{}^{-1}$s and are measures of the membrane fluidity sensed by the ASL (the rotational diffusion of ASL). As with LLMs, the zero-intercept values match those measured experimentally.

In Fig. 2D, the β_{obs} parameters obtained for cortical and nuclear LLMs are plotted versus the air fractions. This analysis clearly indicates that the heterogeneity of the membrane fluidity sensed by molecular oxygen is significantly greater in nuclear IMs than in cortical IMs. The β_Ws obtained by fitting β_{obs} data points to Eq. (3) are 0.724 ± 0.0125 and 0.407±0.0143 for cortical IMs and nuclear IMs, respectively.

3.4. Distribution of spin-lattice relaxation rates of ASL in cortical and nuclear LLMs and IMs

The probability density distributions for the $T_{1N2}{}^{-1}$s of ASL in the investigated membranes were constructed as described in [methods] using fitted parameter from Sec. 3.3. (Fig. 2). In Fig. 3, in addition to the probability density distributions, we indicated regions of $T_{1N2}{}^{-1}$s where appropriate percentiles of possible rates are located using box-and-whiskers plots. The LLMs are represented by single lines because no distributions of $T_{1N2}{}^{-1}$ exist in these samples. The lipid exchange within the ASL environment seems to be sufficiently faster than the relaxation via rotational diffusion; thus, only a single relaxation rate is visible. Nonetheless, cortical LLMs are more fluid than nuclear LLMs, as expected from Chol-to-PL ratios and age-related depletion of unsaturated PLs in nuclear membranes (Estrada and Yappert, 2004).

The major conclusion from these results is that, because LLMs are characterized by a single $T_{1N2}{}^{-1}$ that are faster than their corresponding IMs, the integral and peripheral proteins in IMs create a variety of rigid environments that have a low lipid exchange constant between domains, which contributes to the detected heterogeneity of the ASL rotational diffusion. Additionally, the $T_{1N2}{}^{-1}$s in intact membranes of the successive layers of fiber cells may be different enough to contribute to the observed heterogeneity. The extent of each effect will be investigated in future work. The $T_{1N2}{}^{-1}$s for cortical and nuclear LLMs are faster than at least 75% of $T_{1N2}{}^{-1}$s that can be found in their corresponding IMs. (Very fluid environments should be associated with such fast rates in IMs.) The increased protein content in nuclear IMs compared with that in cortical LLMs corresponds to the wider and more rigid distribution of $T_{1N2}{}^{-1}$s. In IMs, 70% of the of cortical $T_{1N2}{}^{-1}$s density has values between 0.27 μs^{-1} and 0.37 μs^{-1}, and another 20% is distributed as a long tail up to 0.72 μs^{-1}. With the decrease of the lipid-to-protein ratio from 11.5 in cortical IMs to 2.24 in nuclear IMs, the width of the bulk 70% of the $T_{1N2}{}^{-1}$s density has values between 0.16 μs^{-1} and 0.30 μs^{-1}. The long 20% tail distribution also widened up to 0.79 μs^{-1}.

3.5. Distribution of oxygen transport parameters in cortical and nuclear LLMs and IMs

The probability density distribution and subsequent cumulative probability distributions of Ws in cortical and nuclear LLMs and IMs were constructed to examine the difference in values of the oxygen transport parameter among the samples. Cumulative results are presented in Fig. 4 as box-and-whiskers plots with probability density distribution functions for each sample for reference.

The distributions of Ws in cortical and nuclear LLMs are surprisingly similar despite their considerable differences in Chol-to-PL ratios and $T_{1N2}{}^{-1}$ rates. In both samples 75% of the density is distributed between approximately 2 μs^{-1} and 4 μs^{-1}, and another 20% extends to 10 μs^{-1}. Because W is a function of the oxygen diffusion-concentration product, it is possible that the difference in PL types and Chol compositions lands ASL in similar environments regardless of the Chol-to-PL ratio. In our previous publications, we detected no heterogeneity of Ws in membranes made from the total lipids extracted from whole porcine lens (Raguz et al., 2008) or in separated cortical porcine LLMs (Mainali et al., 2012a). This slight heterogeneity might have been missed because the goodness of fit was estimated visually based on the residual. Using the SEF allows us to detect heterogeneity where the double exponential fit might have missed it. Mainali 2012 (Mainali et al., 2012a) reported the presence of some amount of W with the value of 0.5 μs^{-1} in porcine nuclear LLMs; no such low value is present in the current distributions or when fitted to double-exponential function.

Comparison of results obtained for IMs with those obtained for LLMs clearly indicates that the presence of integral and peripheral proteins creates lipid environments in IMs with low ASL Ws. In cortical IMs, 70% of the W distribution extends from 0.95 μs^{-1} to 4.23 μs^{-1}, and another 20% stretches all the way to 12.5 μs^{-1}. The effect is even more pronounced in nuclear IMs where the slowest 5% of the density has rates below 0.15 μs^{-1}, and the slowest 75% below 3.25 μs^{-1}. Comparison of the distribution of Ws between cortical and nuclear IMs indicates that oxygen diffusion-concentration products in nuclear IMs are suppressed by the presence of integral and peripheral membrane proteins much stronger than in cortical IMs. This can be explained by the fact that nuclear IMs are composed of a greater fraction of integral and peripheral proteins (Grami et al., 2005; Tang and Borchman, 1998)which induce formation of lipid domains with very low oxygen accessibility. All the presented data were obtained with spin labels located in different membrane environments. This probe approach permits measurement of collision rates of molecular oxygen with the nitroxide moiety of spin labels, and calculation of the product of the local oxygen diffusion coefficient and the local oxygen concentration. Separation of this product into component factors, diffusion and solubility, is not possible.

$T_{1N2}{}^{-1}$ measurements show membrane fluidity and the heterogeneity sensed by lipid spin labels based on their rotational diffusion, and Ws measurements report membrane fluidity and the heterogeneity through the oxygen diffusion-concentration product in the membrane (by movement and solubility of small probe molecules). Both methods complement each other. A comparison of Figs. 3 and 4 indicates that the Ws method is more than an order of magnitude more sensitive than the $T_{1N2}{}^{-1}$s (in both methods, the measured values are spin-lattice relaxation rates).

We previously demonstrated that the T_{1str}^{-1} and β parameters obtained from the SEF analysis of SR EPR signals coming from spin-labeled deoxygenated cortical and nuclear fiber cell plasma membranes from porcine eye lenses can be used for a multivariate K-means cluster analysis. This analysis is based on the differences in the separation of indicated parameters coming from samples of different origins. Data presented in Fig. 5 indicate that the separation of these data points increases enormously when $T_{1strobs}^{-1}$s and β_{obs}s obtained for samples equilibrated with air are used to separate them. For deoxygenated samples, T_{1strN2}^{-1} and β_{N2} parameters are relatively close to each other, with a Euclidean distance of 0.104. For samples saturated with air, the separation of $T_{1strobs}^{-1}$s and β_{obs}s parameters increased ~16 times to the value of 1.66.

The separation of SEF parameters reflects differences in the fluidity and heterogeneity of lipids in investigated membranes. Presented in Fig. 5 separation of data points was obtained for membranes of relatively young animals. We expect that parameters obtained from SEF analysis of SR EPR signals coming from human lenses will be clearly separated reflecting age related and health related differences in the organization of lipids in fiber cell membranes.

4. Concluding Remarks and Future Directions

In this paper, we describe the fluidity of the lipid bilayer portion of IMs of the porcine eye lens as detected by ASL using SR EPR spectroscopy with the SEF analysis. The membrane fluidity was reported by the rotational diffusion of ASL and by the oxygen transport parameter (oxygen diffusion-concentration product). Two papers, previously published in the specific methodological journal, introduced this new method to analyze the organization, fluidity, and heterogeneity of complex biological membranes when only the rotational diffusion mode of spin lattice relaxation is considered (Stein et al., 2019), and when rotational diffusion and oxygen collisions contribute to the observed SR signal (Stein and Subczynski, 2020).

The conventional CW EPR technique with the use of lipid spin labels was more broadly used to study the structure of eye lens membranes (Babizhayev et al., 1992; Puskin and Wiese, 1982). Our group has also significant achievements in this direction. We applied PL analog spin labels (n-PC and n-SASL) and Chol analogs ASL and CSL to obtain profiles of the physical properties across membranes and to quantitate the amount of lipids with low and high mobility in cortical and nuclear bovine (Raguz et al., 2009; Widomska et al., 2007), porcine (Mainali et al., 2018, 2012a, 2011b; Raguz et al., 2015b), and human (Mainali et al., 2017b, 2015, 2013b; Raguz et al., 2015a, 2014) eye lens IMs as well as across corresponding LLMsThe CW EPR spectrum of ASL in nuclear IMs (recorded as a first derivative of the absorption EPR spectrum) consistently show two components indicated by two clearly separated maximum splitting. The EPR spectra of ASL in other investigated membranes, namely cortical and nuclear LLMs and cortical IMs, show only one component (one maximum splitting is observed). The appearance of the highly immobilized component in the CW EPR spectrum correlates with the aging of fiber cell membranes (Mainali et al., 2015; Raguz et al., 2015a). Aging also correlates with the increased of fraction of protein in the membrane, and associated with the membrane as reported here and elsewhere

(Borchman et al., 1989; Chandrasekher and Cenedella, 1995), breakdown of gap junction and formation of square arrays and microplacia (Bassnett et al., 2011; Costello et al., 1989) possibly caused by truncation and other modifications of integral membrane proteins (Korlimbinis et al., 2009; Wenke et al., 2015). These processes are insidious and may contribute to the formation of trapped and highly immobilized lipids in a variety of domains throughout the layers of cells represented in a sample. Diversity of membrane organization suggests that each component may contain the less abundant signals that get lost in the total broad-spectrum analysis. We hypothesize that the SR EPR method described here can provide this detailed analysis.

SR EPR in magnetically diluted samples and in the absence of oxygen provides information regarding the rotational diffusion of spin labels that depends on the local membrane fluidity (Mainali et al., 2013a, 2011a). Introduction of oxygen into a sample further informs about the membrane fluidity in terms to concentration/diffusion product of the small hydrophobic molecule (Kusumi et al., 1982). The fluidity of biological membranes affects the function of integral proteins, and membrane barrier properties (Almeida et al., 2005; Sezgin et al., 2017; Spector and Yorek, 1985; Subczynski et al., 2009) that is required to maintain membrane and cell homeostasis. The SR signal is recorded as an exponential-like decay. Observed with aging removal of unsaturated phospholipids (Borchman et al., 2004; Estrada and Yappert, 2004) and increase of Chol-to-PL ratios decreases membrane fluidity and creates formation of more rigid lipid environment (Almeida et al., 2005; Subczynski et al., 2009). Simultaneously, with aging the protein mole fraction is increased by the depletion of phospholipids and the increased binding of peripheral proteins. These processes create gradual rigidification of membranes towards the center of the lens. Because components of the multi-exponential decay are non-orthogonal, their numbers and values are difficult to determine (Smith et al., 1976). It is a common practice to fit such signals to double- or triple-exponential decay function and to assign specific values of decay times to select two or three domains, as we did in our previous publications using similar samples. Another method is to report the weighted averages of the two components, as is done in many similar spectroscopies and where stretched exponential application function was also used such as fluorescence life time imaging (Benny Lee et al., 2001) nuclear magnetic imaging (Bennett et al., 2003).

The use of the SEF to analyze a multi-exponential decay SR signal that consists of an undefined number of relaxation constants provides two fitting parameters, the characteristic or stretched spin-lattice relaxation rate T_{1str}^{-1} and the heterogeneity parameter β. If β is 1, then the signal comes from a signal exponential decay. If β is less than 1, this parameter is used to construct the continuous density probability distribution of all possible rates (see schematic explanation in Fig. 1 of (Stein and Subczynski, 2020)). Such distribution removes the necessity of estimating the number of rate constants and allows the rate to be treated as a continuous variable. The clear advantage of this treatment over double exponential is that instead of having only two fixed values a probability of finding any a range of values may be determined. This is convenient for complex biological specimens such as the eye lens membranes, where various domains from an individual fiber cell exist within a membrane, and the domains from different layers of fiber cells may also be different in physical properties measured by SR EPR. Of course, in a continuous distribution, the probability of

any single rate is nil. Instead, the probability of a range of rates must be determined. A range of a certain width under the mode of the distribution will have a higher probability and, therefore, is the larger component of the signal than a range of the same width under the long tail of the distribution. Another important factor to consider is that the distribution is determined by the inverse Laplace transform of the SEF, which is unimodal and has a long tail; this idealized shape may conceal finer details such as the existence of smaller modes.

The exciting application of the SEF is to use the fitting parameters (T_{1str}^{-1}, β) for a multivariate cluster analysis of stretched-exponential data from complex IMs as is demonstrated in (Stein et al., 2019). As demonstrated in Fig. 5, the separation of data points used for cluster analysis increases enormously for samples equilibrated with air. For deoxygenated samples, the T_{1strN2}^{-1} and β_{N2} parameters are relatively close to each other, with a Euclidean distance of 0.11. For samples saturated with air, the separation of the $T_{1strobs}^{-1}$ and β_{obs} parameters increases by an order of magnitude to the value of a Euclidean distance of 1.37. The oxygen-enhanced sensitivity of the advanced SR EPR technique, together with the SEF analysis, makes it possible to obtain measurements on membranes separated from a single human lens samples volume as small as 30 nL to150 nL. Also, it permits the health history of the donor to be considered in the data analysis. We believe that the air-enhanced multivariate K-means cluster analysis of samples from different human populations and with different health histories should help elucidate predispositions for cataract formation.

Here, we show the general abilities of the SR EPR spin-labeling method with the SEF analysis in studies of IMs isolated from the cortex and nucleus of porcine eye lenses. We also indicate future directions in development and applications of this method. The next step will be to apply of this method to study IMs from human eye lenses.

Acknowledgements

Research reported in this publication was supported by the National Eye Institute of the National Institutes of Health under award number R01 EY015526. The content is solely the responsibility of the authors and does not necessarily represent the official views of the National Institutes of Health.

References

Almeida PFF, Pokorny A, Hinderliter A, 2005. Thermodynamics of membrane domains. Biochimica et Biophysica Acta - Biomembranes 1720, 1–13. 10.1016/j.bbamem.2005.12.004

Altenbach C, Froncisz W, Hyde JS, Hubbell WL, 1989. Conformation of spin-labeled melittin at membrane surfaces investigated by pulse saturation recovery and continuous wave power saturation electron paramagnetic resonance. Biophysical Journal 56, 1183–1191. 10.1016/S0006-3495(89)82765-1 [PubMed: 2558734]

Ashikawa I, Yin JJ, Subczynski WK, Hyde JS, Kouyama T, Kusumi A, 1994. Molecular Organization and Dynamics in Bacteriorhodopsin-Rich Reconstituted Membranes: Discrimination of Lipid Environments by the Oxygen Transport Parameter Using a Pulse ESR Spin-Labeling Technique. Biochemistry 33, 4947–4952. 10.1021/bi00182a025 [PubMed: 8161556]

Babizhayev MA, Dainyak BA, Maxina AH, 1992. ESR spin label and ultrastructural monitoring of protein-lipid interactions in the lends fiber-cell plasma membranes in relation to human ageing and cataractogenesis. Mechanisms of Ageing and Development 64, 133–147. 10.1016/0047-6374(92)90102-J [PubMed: 1321312]

Bassnett S, Costello MJ, 2017. The cause and consequence of fiber cell compaction in the vertebrate lens. Experimental Eye Research 156, 50–57. 10.1016/j.exer.2016.03.009 [PubMed: 26992780]

Bassnett S, Shi Y, Vrensen GFJM, 2011. Biological glass: Structural determinants of eye lens transparency. Philosophical Transactions of the Royal Society B: Biological Sciences 366, 1250–1264. 10.1098/rstb.2010.0302 [PubMed: 21402584]

Bennett KM, Schmainda KM, Bennett R, Rowe DB, Lu H, Hyde JS, 2003. Characterization of continuously distributed cortical water diffusion rates with a stretched-exponential model. Magnetic Resonance in Medicine 50, 727–734. 10.1002/mrm.10581 [PubMed: 14523958]

Benny Lee KC, Siegel J, Webb SED, Lévêque-Fort S, Cole MJ, Jones R, Dowling K, Lever MJ, French PMW, 2001. Application of the stretched exponential function to fluorescence lifetime imaging. Biophysical Journal 81, 1265–1274. 10.1016/s0006-3495(01)75784-0 [PubMed: 11509343]

Bieri VG, Hoelzl Wallach DF, 1975. Variations of lipid-protein interactions in erythrocyte ghosts as a function of temperature and pH in physiological and non-physiological ranges. A study using paramagnetic quenching of protein fluorescence by nitroxide lipid analogues. BBA - Biomembranes 406, 415–423. 10.1016/0005-2736(75)90020-6 [PubMed: 241415]

Bloemendal H, Zweers A, Vermorken F, Dunia I, Benedetti EL, 1972. The plasma membranes of eye lens fibres. Biochemical and structural characterization. Cell Differentiation 1, 91–106. 10.1016/0045-6039(72)90032-2 [PubMed: 4275925]

Borchman D, Delamere NA, McCauley LA, Paterson CA, 1989. Studies on the distribution of cholesterol, phospholipid, and protein in the human and bovine lens, in: Lens and Eye Toxicity Research. pp. 703–724. [PubMed: 2487279]

Borchman D, Yappert MC, 2010. Lipids and the ocular lens. Journal of Lipid Research 51, 2473–2488. 10.1194/jlr.R004119 [PubMed: 20407021]

Borchman D, Yappert MC, Afzal M, 2004. Lens lipids and maximum lifespan. Experimental Eye Research 79, 761–768. 10.1016/j.exer.2004.04.004 [PubMed: 15642313]

Buzhynskyy N, Sens P, Behar-Cohen F, Scheuring S, 2011. Eye lens membrane junctional microdomains: A comparison between healthy and pathological cases. New Journal of Physics 13, 085016. 10.1088/1367-2630/13/8/085016

Cenedella RJ, Fleschner CR, 1992. Selective association of crystallins with Lens “native” membrane during dynamic cataractogenesis. Current Eye Research 11, 801–815. 10.3109/02713689209000753 [PubMed: 1424724]

Chandrasekher G, Cenedella RJ, 1995. Protein associated with human lens “native” membrane during aging and cataract formation. Experimental Eye Research 60, 707–717. 10.1016/S0014-4835(05)80012-0 [PubMed: 7641853]

Costello MJ, McIntosh TJ, Robertson JD, 1989. Distribution of gap junctions and square array junctions in the mammalian lens. Investigative Ophthalmology and Visual Science 30, 975–989. [PubMed: 2722452]

Deeley JM, Mitchell TW, Wei X, Korth J, Nealon JR, Blanksby SJ, Truscott RJW, 2008. Human lens lipids differ markedly from those of commonly used experimental animals. Biochimica et Biophysica Acta - Molecular and Cell Biology of Lipids 1781, 288–298. 10.1016/j.bbalip.2008.04.002

Dupuy AD, Engelman DM, 2008. Protein area occupancy at the center of the red blood cell membrane. Proceedings of the National Academy of Sciences of the United States of America 105, 2848–2852. 10.1073/pnas.0712379105 [PubMed: 18287056]

Estrada R, Yappert MC, 2004. Regional phospholipid analysis of porcine lens membranes by matrix-assisted laser desorption/ionization time-of-flight mass spectrometry, in: Journal of Mass Spectrometry. pp. 1531–1540. 10.1002/jms.759 [PubMed: 15578747]

Grami V, Marrero Y, Huang L, Tang D, Yappert MC, Borchman D, 2005. α-Crystallin binding in vitro to lipids from clear human lenses. Experimental Eye Research 81, 138–146. 10.1016/j.exer.2004.12.014 [PubMed: 15967437]

Hubbell WL, McConnel HM, 1971. Molecular Motion in Spin-Labeledla Phospholipids and Membranes. Journal of the American Chemical Society 93, 314–326. 10.1021/ja00731a005 [PubMed: 5541516]

Johnston DC, 2006. Stretched exponential relaxation arising from a continuous sum of exponential decays. Physical Review B - Condensed Matter and Materials Physics 74, 184430. 10.1103/PhysRevB.74.184430

Kawasaki K, Yin JJ, Subczynski WK, Hyde JS, Kusumi A, 2001. Pulse EPR detection of lipid exchange between protein-rich raft and bulk domains in the membrane: Methodology development and its application to studies of influenza viral membrane. Biophysical Journal 80, 738–48. 10.1016/S0006-3495(01)76053-5 [PubMed: 11159441]

Korlimbinis A, Berry Y, Thibault D, Schey KL, Truscott RJW, 2009. Protein aging: Truncation of aquaporin 0 in human lens regions is a continuous age-dependent process. Experimental Eye Research 88, 966–973. 10.1016/j.exer.2008.12.008 [PubMed: 19135052]

Kusumi A, Subczynski WK, Pasenkiewicz-Gierula M, Hyde JS, Merkle H, 1986. Spin-label studies on phosphatidylcholine-cholesterol membranes: effects of alkyl chain length and unsaturation in the fluid phase. BBA - Biomembranes 854, 307–317. 10.1016/0005-2736(86)90124-0 [PubMed: 3002470]

Kusumi A, Subczynski WK, Hyde JS, 1982. Oxygen transport parameter in membranes as deduced by saturation recovery measurements of spin-lattice relaxation times of spin labels. Proceedings of the National Academy of Sciences of the United States of America 79, 1854–1858. 10.1073/pnas.79.6.1854 [PubMed: 6952236]

Mailer C, Nielsen RD, Robinson BH, 2005. Explanation of spin-lattice relaxation rates of spin labels obtained with multifrequency saturation recovery EPR. Journal of Physical Chemistry A 109, 4049–4061. 10.1021/jp044671l

Mainali L, Camenisch TG, Hyde JS, Subczynski WK, 2017a. Saturation Recovery EPR Spin-Labeling Method for Quantification of Lipids in Biological Membrane Domains. Applied Magnetic Resonance 48, 1355–1373. 10.1007/s00723-017-0921-x [PubMed: 29805201]

Mainali L, Feix JB, Hyde JS, Subczynski WK, 2011a. Membrane fluidity profiles as deduced by saturation-recovery EPR measurements of spin-lattice relaxation times of spin labels. Journal of Magnetic Resonance 212, 418–425. 10.1016/j.jmr.2011.07.022 [PubMed: 21868272]

Mainali L, Hyde JS, Subczynski WK, 2013a. Using spin-label W-band EPR to study membrane fluidity profiles in samples of small volume. Journal of Magnetic Resonance 226, 35–44. 10.1016/j.jmr.2012.11.001 [PubMed: 23207176]

Mainali L, O'Brien WJ, Hyde JS, Subczynski WK, 2018. Detection of Pure Cholesterol Bilayer Domains in Biological Membranes Overloaded with Cholesterol: Methodology Development and its Application to Porcine Lens Membrane Studies, in: Biophysical Journal. pp. 449a–449a. 10.1016/j.bpj.2017.11.2485

Mainali L, Raguz M, Camenisch TG, Hyde JS, Subczynski WK, 2011b. Spin-label saturation-recovery EPR at W-band: Applications to eye lens lipid membranes. Journal of Magnetic Resonance 212, 86–94. 10.1016/j.jmr.2011.06.014 [PubMed: 21745756]

Mainali L, Raguz M, O'Brien WJ, Subczynski WK, 2017b. Changes in the Properties and Organization of Human Lens Lipid Membranes Occurring with Age. Current Eye Research 42, 721–731. 10.1080/02713683.2016.1231325 [PubMed: 27791387]

Mainali L, Raguz M, O'Brien WJ, Subczynski WK, 2015. Properties of membranes derived from the total lipids extracted from clear and cataractous lenses of 61–70-year-old human donors. European Biophysics Journal 44, 91–102. 10.1007/s00249-014-1004-7 [PubMed: 25502634]

Mainali L, Raguz M, O'Brien WJ, Subczynski WK, 2013b. Properties of membranes derived from the total lipids extracted from the human lens cortex and nucleus. Biochimica et Biophysica Acta - Biomembranes 1828, 1432–1440. 10.1016/j.bbamem.2013.02.006

Mainali L, Raguz M, O'Brien WJ, Subczynski WK, 2012a. Properties of fiber cell plasma membranes isolated from the cortex and nucleus of the porcine eye lens. Experimental Eye Research 97, 117–129. 10.1016/j.exer.2012.01.012 [PubMed: 22326289]

Mainali L, Raguz M, Subczynski WK, 2013c. Formation of cholesterol bilayer domains precedes formation of cholesterol crystals in cholesterol/dimyristoylphosphatidylcholine membranes: EPR and DSC studies. Journal of Physical Chemistry B 117, 8994–9003. 10.1021/jp402394m

Mainali L, Raguz M, Subczynski WK, 2012b. Phases and domains in sphingomyelin-cholesterol membranes: Structure and properties using EPR spin-labeling methods. European Biophysics Journal 41, 147–159. 10.1007/s00249-011-0766-4 [PubMed: 22033879]

Marsh D, 2018. Molecular order and T1-relaxation, cross-relaxation in nitroxide spin labels. Journal of Magnetic Resonance 290, 38–45. 10.1016/J.JMR.2018.02.020 [PubMed: 29550514]

Páli T, Kóta Z, 2019. Studying Lipid–Protein Interactions with Electron Paramagnetic Resonance Spectroscopy of Spin-Labeled Lipids, in: Kleinschmidt J (Ed.), Methods in Molecular Biology. Humana, New York, NY, pp. 529–561. 10.1007/978-1-4939-9512-7_22

Puskin JS, Wiese MB, 1982. A spin label study of human lens membranes. Experimental Eye Research 35, 251–258. 10.1016/S0014-4835(82)80049-3 [PubMed: 6288425]

Raguz M, Mainali L, O'Brien WJ, Subczynski WK, 2015a. Lipid domains in intact fiber-cell plasma membranes isolated from cortical and nuclear regions of human eye lenses of donors from different age groups. Experimental Eye Research 132, 78–90. 10.1016/j.exer.2015.01.018 [PubMed: 25617680]

Raguz M, Mainali L, O'Brien WJ, Subczynski WK, 2015b. Amounts of phospholipids and cholesterol in lipid domains formed in intact lens membranes: Methodology development and its application to studies of porcine lens membranes. Experimental Eye Research 140, 179–186. 10.1016/j.exer.2015.09.006 [PubMed: 26384651]

Raguz M, Mainali L, O'Brien WJ, Subczynski WK, 2014. Lipid-protein interactions in plasma membranes of fiber cells isolated from the human eye lens. Experimental Eye Research 120, 138–151. 10.1016/j.exer.2014.01.018 [PubMed: 24486794]

Raguz M, Mainali L, Widomska J, Subczynski WK, 2011a. Using spin-label electron paramagnetic resonance (EPR) to discriminate and characterize the cholesterol bilayer domain. Chemistry and Physics of Lipids 164, 819–829. 10.1016/j.chemphyslip.2011.08.001 [PubMed: 21855534]

Raguz M, Mainali L, Widomska J, Subczynski WK, 2011b. The immiscible cholesterol bilayer domain exists as an integral part of phospholipid bilayer membranes. Biochimica et Biophysica Acta - Biomembranes 1808, 1072–1080. 10.1016/j.bbamem.2010.12.019

Raguz M, Widomska J, Dillon J, Gaillard ER, Subczynski WK, 2009. Physical properties of the lipid bilayer membrane made of cortical and nuclear bovine lens lipids: EPR spin-labeling studies. Biochimica et Biophysica Acta - Biomembranes 1788, 2380–2388. 10.1016/j.bbamem.2009.09.005

Raguz M, Widomska J, Dillon J, Gaillard ER, Subczynski WK, 2008. Characterization of lipid domains in reconstituted porcine lens membranes using EPR spin-labeling approaches. Biochimica et Biophysica Acta - Biomembranes 1778, 1079–1090. 10.1016/j.bbamem.2008.01.024

Robinson BH, Haas DA, Mailer C, 1994. Molecular dynamics in liquids: Spin-lattice relaxation of nitroxide spin labels. Science 263, 490–493. 10.1126/science.8290958 [PubMed: 8290958]

Rujoi M, Jin J, Borchman D, Tang D, Yappert MC, 2003. Isolation and lipid characterization of cholesterol-enriched fractions in cortical and nuclear human lens fibers. Investigative Ophthalmology and Visual Science 44, 1634–1642. 10.1167/iovs.02-0786 [PubMed: 12657603]

Sezgin E, Levental I, Mayor S, Eggeling C, 2017. The mystery of membrane organization: Composition, regulation and roles of lipid rafts. Nature Reviews Molecular Cell Biology 18, 361–374. 10.1038/nrm.2017.16 [PubMed: 28356571]

Smith MR, Cohn-Sfetcu S, Buckmaster HA, 1976. Decomposition of multicomponent exponential decays by spectral analytic techniques. Technometrics 18, 567–482. 10.1080/00401706.1976.10489479

Song S, Landsbury A, Dahm R, Liu Y, Zhang Q, Quinlan RA, 2009. Functions of the intermediate filament cytoskeleton in the eye lens. The Journal of Clinical Investigation 119, 1837–1848. 10.1172/JCI38277. [PubMed: 19587458]

Spector AA, Yorek MA, 1985. Membrane lipid composition and cellular function. Journal of Lipid Research 26, 1015–1035. 10.1016/S0022-2275(20)34276-0 [PubMed: 3906008]

Stein N, Mainali L, Hyde JSJS, Subczynski WK, 2019. Characterization of the Distribution of Spin–Lattice Relaxation Rates of Lipid Spin Labels in Fiber Cell Plasma Membranes of Eye Lenses with a Stretched Exponential Function. Applied Magnetic Resonance 50, 903–918. 10.1007/s00723-019-01119-7 [PubMed: 31244509]

Stein N, Subczynski WK, 2020. Oxygen Transport Parameter in Plasma Membrane of Eye Lens Fiber Cells by Saturation Recovery EPR. Applied Magnetic Resonance. 10.1007/s00723-020-01237-7

Su SP, McArthur JD, Truscott RJW, Aquilina JA, 2011. Truncation, cross-linking and interaction of crystallins and intermediate filament proteins in the aging human lens. Biochimica et Biophysica Acta - Proteins and Proteomics 1814, 647–656. 10.1016/j.bbapap.2011.03.014

Subczynski WK, Felix CC, Klug CS, Hyde JS, 2005. Concentration by centrifugation for gas exchange EPR oximetry measurements with loop-gap resonators. Journal of Magnetic Resonance 176, 244–248. 10.1016/j.jmr.2005.06.011 [PubMed: 16040261]

Subczynski WK, Hopwood LE, Hyde JS, 1992. Is the mammalian cell plasma membrane a barrier to oxygen transport? Journal of General Physiology 100, 69–87. 10.1085/jgp.100.1.69

Subczynski WK, Hyde JS, Kusumi A, 1989. Oxygen permeability of phosphatidylcholine-cholesterol membranes. Proceedings of the National Academy of Sciences of the United States of America 86, 4474–4478. 10.1073/pnas.86.12.4474 [PubMed: 2543978]

Subczynski WK, Hyde JS, Kusumi A, Subczynski WK, Kusumi A, 1991. Effect of Alkyl Chain Unsaturation and Cholesterol Intercalation on Oxygen Transport in Membranes: A Pulse ESR Spin Labeling Study. Biochemistry 30, 8578–8590. 10.1021/bi00099a013 [PubMed: 1653601]

Subczynski, Witold K, Pasenkiewicz-Gierula M, Widomska, • Justyna, Mainali L, Marija Raguz, •, 2017. High Cholesterol/Low Cholesterol: Effects in Biological Membranes: A Review. Cell Biochemistry and Biophysics 75, 369–385. 10.1007/s12013-017-0792-7 [PubMed: 28417231]

Subczynski WK, Raguz M, Widomska J, 2010. Studying lipid organization in biological membranes using liposomes and EPR spin labeling. Methods in molecular biology (Clifton, N.J.) 606, 247–269. 10.1007/978-1-60761-447-0_18

Subczynski WK, Widomska J, Feix JB, 2009. Physical properties of lipid bilayers from EPR spin labeling and their influence on chemical reactions in a membrane environment. Free Radical Biology and Medicine 46, 707–718. 10.1016/j.freeradbiomed.2008.11.024 [PubMed: 19111611]

Subczynski WK, Widomska J, Mainali L, 2017. Factors determining the oxygen permeability of biological membranes: Oxygen transport across eye lens fiber-cell plasma membranes: Oxygen transport across eye lens fiber-cell plasma membranes, in: Halpern H, LaManna JC, Harrison DK, Epel B (Eds.), Oxygen Transport to Tissue XXXIX. Advances in Experimental Medicine and Biology Vol. 977. Springer, pp. 27–34. 10.1007/978-3-319-55231-6

Subczynski WK, Widomska J, Wisniewska A, Kusumi A, 2007a. Saturation-recovery electron paramagnetic resonance discrimination by oxygen transport (DOT) method for characterizing membrane domains, in: McIntosh TJ (Ed.), Methods in Molecular Biology. Humana Press, pp. 143–157. 10.1007/978-1-59745-513-8_11

Subczynski WK, Wisniewska A, Hyde JS, Kusumi A, 2007b. Three-dimensional dynamic structure of the liquid-ordered domain in lipid membranes as examined by pulse-EPR oxygen probing. Biophysical Journal 92, 1573–1584. 10.1529/biophysj.106.097568 [PubMed: 17142270]

Tang D, Borchman D, 1998. Temperature induced structural changes of β-crystallin and sphingomyelin binding. Experimental Eye Research 67, 113–118. 10.1006/exer.1998.0497 [PubMed: 9702184]

Truscott RJW, Comte-Walters S, Ablonczy Z, Schwacke JH, Berry Y, Korlimbinis A, Friedrich MG, Schey KL, 2011. Tight binding of proteins to membranes from older human cells. Age 33, 543–555. 10.1007/s11357-010-9198-9 [PubMed: 21181282]

Wang Z, Han J, David LL, Schey KL, 2013. Proteomics and phosphoproteomics analysis of human lens fiber cell membranes. Investigative Ophthalmology and Visual Science 54, 1135–1143. 10.1167/iovs.12-11168 [PubMed: 23349431]

Warren GB, Houslay MD, Metcalfe JC, Birdsall NJM, 1975. Cholesterol is excluded from the phospholipid annulus surrounding an active calcium transport protein. Nature 255, 684–687. 10.1038/255684a0 [PubMed: 124402]

Wenke JL, Rose KL, Spraggins JM, Schey KL, 2015. MALDI imaging mass spectrometry spatially maps age- related deamidation and truncation of human lens aquaporin-0. Investigative Ophthalmology and Visual Science 56, 7398–7405. 10.1167/iovs.15-18117 [PubMed: 26574799]

Widomska J, Raguz M, Subczynski WK, 2007. Oxygen permeability of the lipid bilayer membrane made of calf lens lipids. Biochimica et Biophysica Acta - Biomembranes 1768, 2635–2645. 10.1016/j.bbamem.2007.06.018

Wisniewska A, Subczynski WK, 2008. The liquid-ordered phase in sphingomyelin-cholesterol membranes as detected by the discrimination by oxygen transport (DOT) method. Cellular and Molecular Biology Letters 13, 430–451. 10.2478/s11658-008-0012-y [PubMed: 18385950]

Yappert MC, Rujoi M, Borchman D, Vorobyov I, Estrada R, 2003. Glycero- versus sphingo-phospholipids: Correlations with human and non-human mammalian lens growth. Experimental Eye Research 76, 725–734. 10.1016/S0014-4835(03)00051-4 [PubMed: 12742355]

Yin JJ, Pasenkiewicz-Gierula M, Hyde JS, 1987. Lateral diffusion of lipids in membranes by pulse saturation recovery electron spin resonance. Proceedings of the National Academy of Sciences of the United States of America 84, 964–968. 10.1073/pnas.84.4.964 [PubMed: 3029766]

Highlights:

- Distribution of the rotational diffusion of cholesterol in eye lens membranes
- Distribution of the oxygen transport parameter in eye lens membranes
- Application of stretched exponential analysis to study membrane dynamics

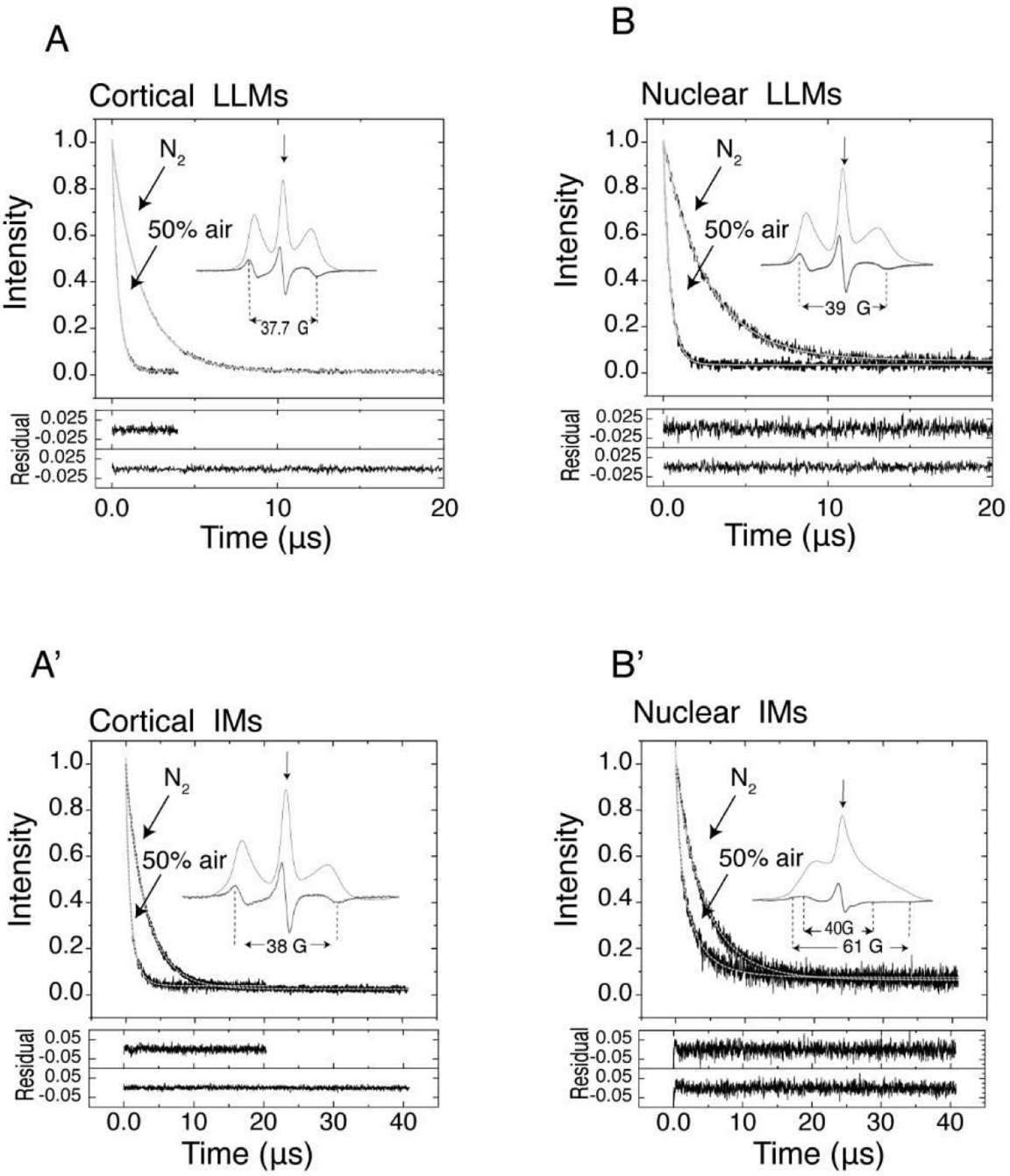

Fig. 1.

Representative SR signals with fitted curves and residuals (the experimental signal minus the fitted curve) for ASL in deoxygenated cortical and nuclear LLMs and IMs and in membranes equilibrated with 50% air. SR signals presented in Fig. 1, which were obtained at different air fractions in the equilibrating gas mixture, were fitted to Eq. (1). The fitting parameters $T_{1\text{strobs}}^{-1}$ and β_{obs} are displayed in Fig. 2. Inserts show the CW EPR spectra of ASL in deoxygenated membranes (thick lines) also displayed as absorption spectra (thin lines). The position of certain peaks in the EPR spectra was evaluated by monitoring the

spectra at higher receiver gains and higher modulation amplitudes. The saturating microwave pump pulse is located at the field position of maximum intensity in the EPR absorption spectrum (indicated by an arrow). The recovery of the signal was recorded at the same field position with a low microwave power. All necessary details are indicated in the appropriate figures.

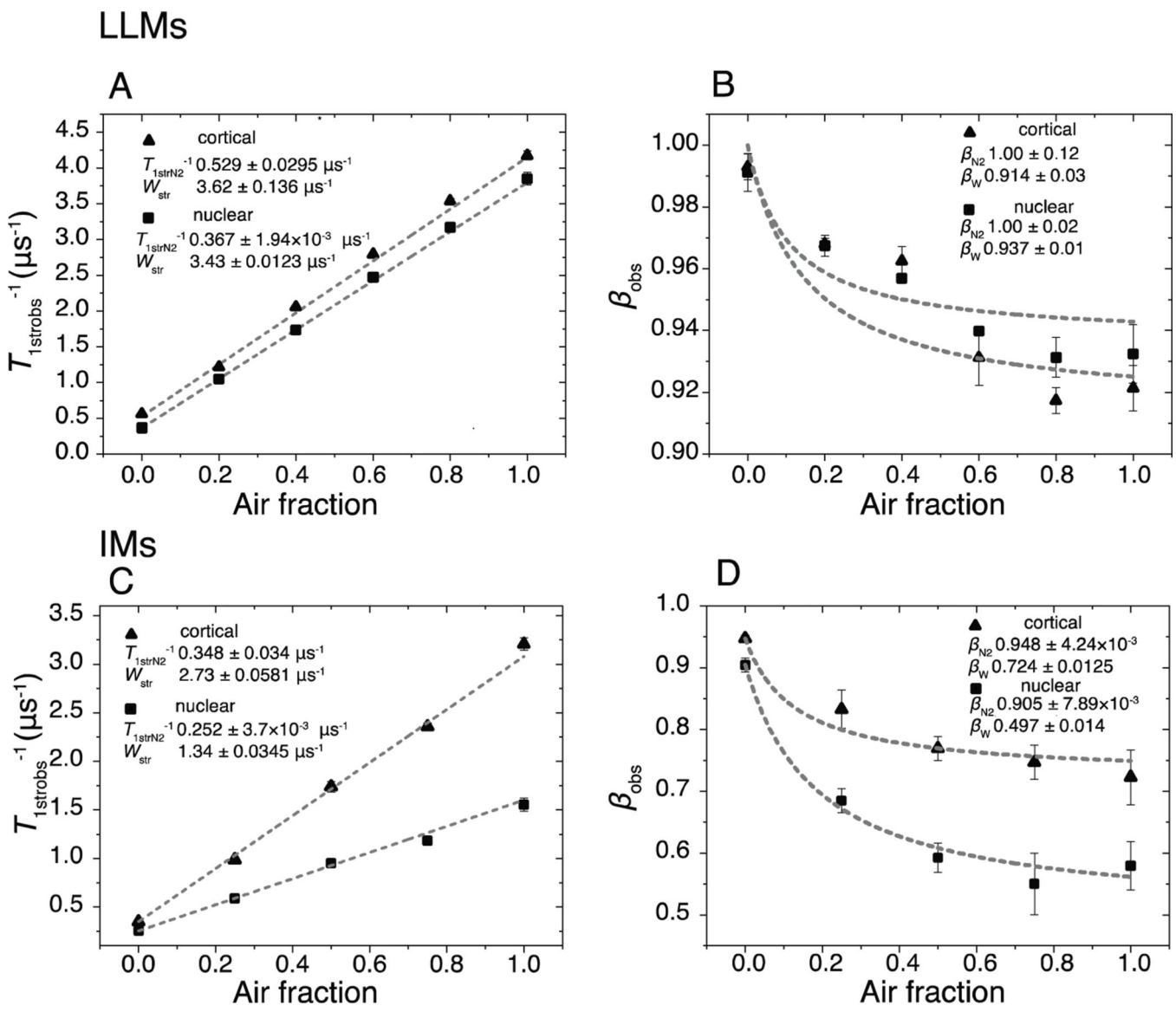

Fig. 2.

In A and B, fitting parameters $T_{1strobs}{}^{-1}$ and β_{obs}, which were obtained from fitting the SR signals of the cortical and nuclear LLMs using Eq. (1), are plotted versus the air fractions at which samples were equilibrated. **A.** The average $T_{1strobs}{}^{-1}$ values from fitting at least three SR signals using Eq. (1) are indicated by black triangles and squares, respectively, for cortical and nuclear LLMs, with vertical bars that represent the standard deviations. The lines are linear fits of these data points. The values following the ± sign are standard errors of the parameters. **B.** The black triangles and black squares are the average values of β_{obs} obtained from at least three SR signals, and the vertical lines correspond to standard deviations. Fits to Eq. 3 are indicated by lines. In C and D, fitting parameters $T_{1strobs}{}^{-1}$ and β_{obs}, which were obtained from fitting the SR signals of the cortical and nuclear IMs using Eq. (1), are plotted versus the air fractions at which samples were equilibrated. **C.** The average $T_{1strobs}{}^{-1}$ values from fitting at least three SR signals using Eq. (1) are indicated by black triangles and squares for cortical and nuclear IMs, respectively, with vertical bars that

represent the standard deviations. The linear fits of these data points with the air fraction are also shown. The values following the ± sign are standard errors of the parameters. **D.** The black triangles and black squares are the average values of β_{obs} obtained from at least three SR signals, and the vertical lines correspond to standard deviations. Fits to Eq. 3 are indicated by lines.

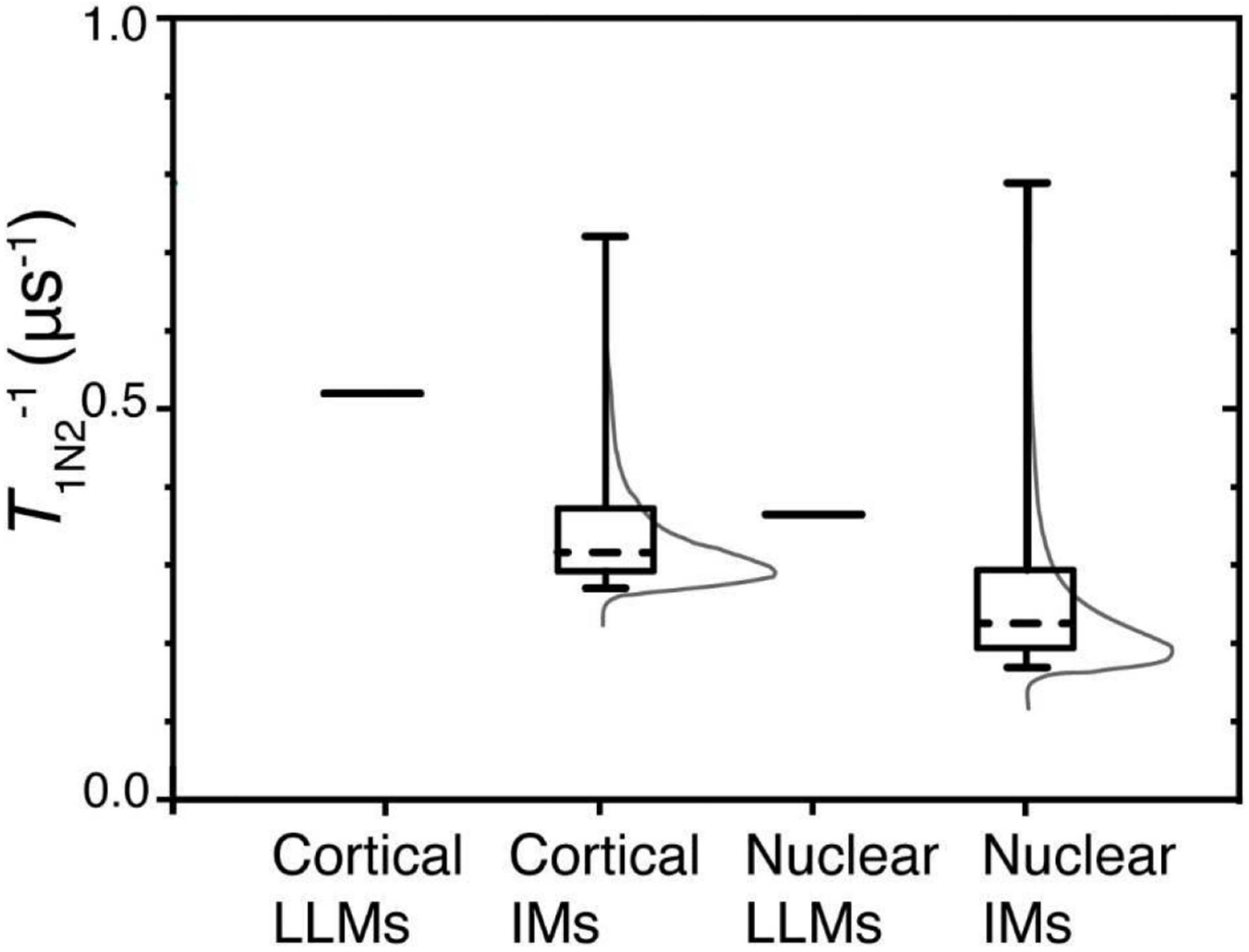

Fig. 3.

Using Laplace transform (Johnston, 2006; Stein et al., 2019) and the fitted parameters $T_{1strN2}{}^{-1}$ and β_{N2}, probability distribution densities of $T_{1N2}{}^{-1}$s were constructed for each sample. These distributions, which are associated with the rotational diffusion of ASL in IMs, are represented by thin gray lines. Rotational diffusions of spin-lattice relaxation rates of ASL in cortical and nuclear LLMs are characterized by a single $T_{1N2}{}^{-1}$ and, for both types of membrane, these distributions are depicted by single lines (delta functions) at $T_{1N2}{}^{-1}$, which are equal to 0.529 μs^{-1} and 0.367 μs^{-1} for cortical and nuclear LLMs, respectively. The rate percentiles were determined from cumulative probability distributions by integrating probability density distributions [First]. The whiskers in Fig. 3 extend from the 5th to 95th percentiles of all possible rates in a given distribution, the boxes extend from the 25th to 75th percentiles, and the dashed lines represent the 50th percentiles of cumulative probability distributions.

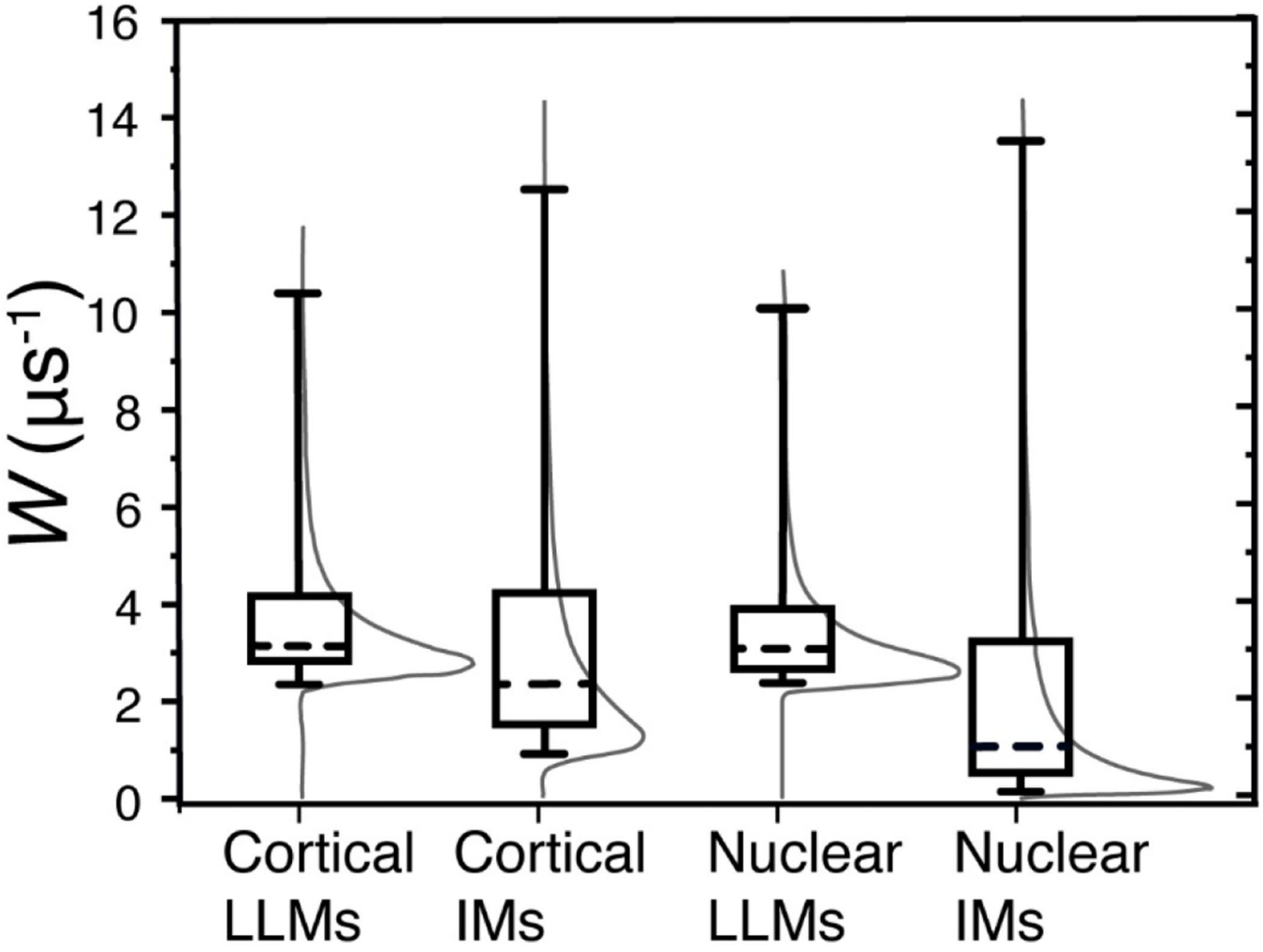

Fig. 4.

The distributions of *W*s in cortical and nuclear IMs and in the LLMs associated with them, they are indicated by thin gray lines. The whiskers (cumulative probability distributions) extend from the 5th to 95th percentile of all possible collision rates in a given sample. The boxes extend from the 25th to 75th percentiles, and the dashed lines represent the 50th percentiles of cumulative probability distributions.

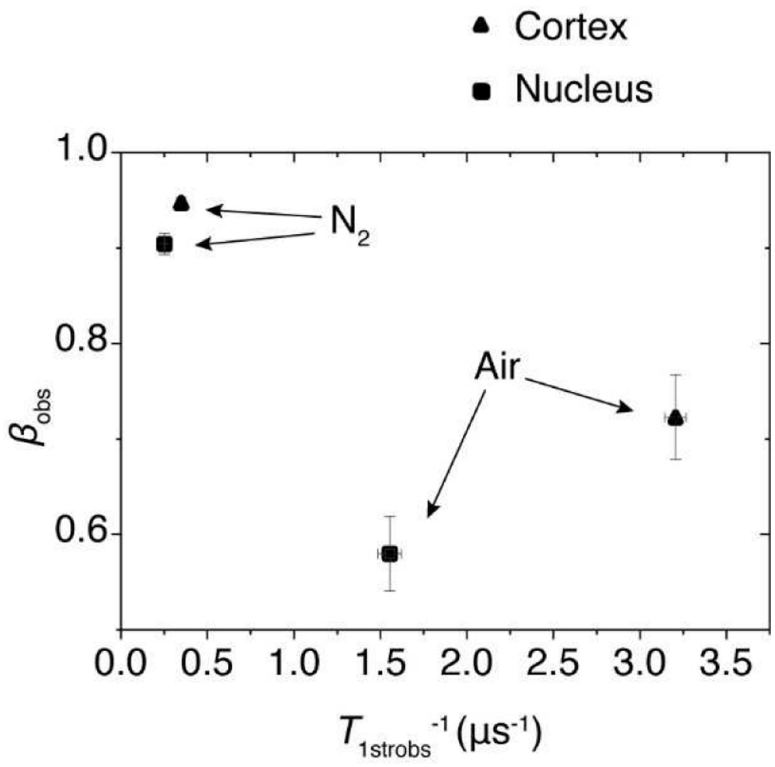

Fig. 5.

Multivariable plot of $T_{1strobs}^{-1}$ and β_{obs} parameters obtained with the SEF analysis of ASL SR signals from IMs for deoxygenated samples and samples equilibrated with air. Data from (▲) cortical IMs and (■) nuclear IMs. The error bars represent the standard deviations.